The Ferredoxin-NADP(H) Reductase from *Rhodobacter capsulatus*: Molecular Structure and Catalytic Mechanism[†,‡]

Isabel Nogués,[§,||] Inmaculada Pérez-Dorado,[||,⊥] Susana Frago,[§] Cristian Bittel,[#] Stephen G. Mayhew,[▽] Carlos Gómez-Moreno,[§] Juan A. Hermoso,[⊥] Milagros Medina,[§] Néstor Cortez,[#] and Néstor Carrillo*[,#]

Departamento de Bioquímica y Biología Molecular y Celular, Facultad de Ciencias, and Institute of Biocomputation and Physics of Complex Systems (BIFI), Universidad de Zaragoza, Zaragoza, Spain, Grupo de Cristalografía Macromolecular y Biología Estructural, Instituto de Química-Física Rocasolano, CSIC Madrid, Madrid, Spain, Instituto de Biología Molecular y Celular de Rosario (IBR), CONICET-Universidad Nacional de Rosario, Rosario, Argentina, and Department of Biochemistry, Conway Institute of Biomolecular and Biomedical Research, University College Dublin, Belfield, Dublin, Ireland

Received May 3, 2005; Revised Manuscript Received July 1, 2005

ABSTRACT: The photosynthetic bacterium *Rhodobacter capsulatus* contains a ferredoxin (flavodoxin)-NADP(H) oxidoreductase (FPR) that catalyzes electron transfer between NADP(H) and ferredoxin or flavodoxin. The structure of the enzyme, determined by X-ray crystallography, contains two domains harboring the FAD and NADP(H) binding sites, as is typical of the FPR structural family. The FAD molecule is in a hairpin conformation in which stacking interactions can be established between the dimethylisoalloxazine and adenine moieties. The midpoint redox potentials of the various transitions undergone by *R. capsulatus* FPR were similar to those reported for their counterparts involved in oxygenic photosynthesis, but its catalytic activity is orders of magnitude lower ($1-2\ s^{-1}$ versus $200-500\ s^{-1}$) as is true for most of its prokaryotic homologues. To identify the mechanistic basis for the slow turnover in the bacterial enzymes, we dissected the *R. capsulatus* FPR reaction into hydride transfer and electron transfer steps, and determined their rates using stopped-flow methods. Hydride exchange between the enzyme and NADP(H) occurred at $30-150\ s^{-1}$, indicating that this half-reaction does not limit FPR activity. In contrast, electron transfer to flavodoxin proceeds at $2.7\ s^{-1}$, in the range of steady-state catalysis. Flavodoxin semiquinone was a better electron acceptor for FPR than oxidized flavodoxin under both single turnover and steady-state conditions. The results indicate that one-electron reduction of oxidized flavodoxin limits the enzyme activity in vitro, and support the notion that flavodoxin oscillates between the semiquinone and fully reduced states when FPR operates in vivo.

Ferredoxin-NADP(H) reductases (FPR or FNR,[1] EC 1.18.1.2) are ubiquitous, monomeric enzymes that contain noncovalently bound FAD as prosthetic group (*1*−*6*). They catalyze the reversible electron exchange between one molecule of NADP(H) and two molecules of the iron−sulfur protein ferredoxin (Fd) or the FMN-containing protein flavodoxin (Fld). The ability of these reductases to mediate electron transfer between obligatory one- (Fd, Fld) and two-electron carriers ($NADP^+$, NADPH), which is so relevant for FNR/FPR function in vivo, stems from the property of the flavin group to oscillate among oxidized, one-electron-reduced (semiquinone) and fully reduced (hydroquinone) states. Interconversion of the three species is facilitated in these flavoenzymes by the relatively small differences existing in the redox potentials for the various one- and two-electron transfer processes (*1*, *4*). The overall reaction can thus be envisaged as consisting of two steps: hydride transfer to or from NADP(H), and electron exchange with the protein partner:

$$NADPH + FPR_{ox} \rightarrow NADP^+ + FPR_{rd} \quad (1)$$

$$FPR_{rd} + 2Fd(Fe^{+3}) \rightarrow FPR_{ox} + 2Fd(Fe^{+2}) \quad (2a)$$

$$FPR_{rd} + 2Fld_{ox} \rightarrow FPR_{ox} + 2Fld_{sq} \quad (2b)$$

or

$$FPR_{rd} + 2Fld_{sq} \rightarrow FPR_{ox} + 2Fld_{rd} \quad (2c)$$

[†] This work was supported by Comisión Interministerial de Ciencia y Tecnología (Grant BIO2004-00279 to M.M.), ANPCyT Argentina (PICT 01-14648 to N. Carrillo), and CONICET Argentina (PEI 6214 to N. Cortez). N. Cortez and N. Carrillo are Staff Members and C.B. is a Fellow of CONICET.

[‡] The coordinates for the structures of FPR were deposited in the Protein Data Bank under accession numbers 2bgi (trigonal form) and 2bgj (monoclinic form).

* To whom correspondence should be addressed. Tel.: 54-341-4350661. Fax: 54-341-4390465. E-mail: carrill@arnet.com.ar.

[§] Universidad de Zaragoza.

[||] I.N. and I.P.-D. have contributed equally to the manuscript, and both should be considered as first author.

[⊥] CSIC Madrid.

[#] CONICET-Universidad Nacional de Rosario.

[▽] University College Dublin.

[1] Abbreviations: Although the acronym FNR was classically used for the photosynthetic ferredoxin(flavodoxin)-NADP(H) reductase from plant and cyanobacteria, the name *fpr* was proposed for the corresponding gene in *E. coli*. We employ the term FPR for the bacterial reductases, while preserving FNR for the plant and cyanobacterial enzymes. Other abbreviations: AMP, adenosine 5′-monophosphate; cyt *c*, cytochrome *c*; dRf, deazariboflavin; Fd, ferredoxin, Fld, flavodoxin; HTG, *n*-heptyl-*β*-D-thioglucoside; P450R, NADPH-cytochrome P450 reductase; rmsd, root-mean-square deviation.

10.1021/bi0508183 CCC: $30.25
Published on Web 08/12/2005

in which the subscripts ox, sq, and rd refer to the oxidized, semiquinone, and hydroquinone forms of the corresponding flavoproteins. The first reductase of this class to be characterized at the structural level was the FNR from spinach chloroplasts, which is made up of two structural domains, each containing approximately 150 amino acids (*7*). The N-terminal region consists of a scaffold of six antiparallel strands, and binds FAD through hydrogen bonds, van der Waals contacts, and stacking interactions. The C-terminal module contains a canonical NADP(H) binding site in a core of five parallel β-strands surrounded by seven α helices (*7*−*9*). Members of the FNR/FPR family have been found in plant and algal plastids, cyanobacteria, proteobacteria, and apicoplasts from obligate intracellular parasites (reviewed in ref *3*). Their distribution matches that of the electron transfer partner Fd, whereas Fld is restricted to prokaryotes and some eukaryotic algae (*10*−*13*). In different organisms including cyanobacteria, Fld synthesis is up-regulated under conditions of nitrogen (*10*, *12*) and/or iron deficit, when the [2Fe-2S] cluster of Fd cannot be assembled (*13*, *14*), or by exposure to oxidants (*14*−*16*). Both Fld *and* FNR/FPR participate in detoxification of reactive oxygen species in aerobic and facultative bacteria (*14*−*18*). In principle, Fld is able to exchange one or two electrons through its flavin group, but potentiometric measurements and identification of transient intermediates suggest that it behaves in vivo as a monoelectronic carrier as does its functional counterpart Fd (*1*−*4*).

When light is the major source of reducing power, as it occurs in organisms displaying oxygenic photosynthesis, the reversible reaction catalyzed by FNR/FPR is displaced toward $NADP^+$ reduction, providing the NADPH needed for CO_2 assimilation and other biosynthetic pathways. Conversely, the ferredoxin reductases present in heterotrophic organisms and tissues operate in reverse, draining reducing equivalents from the cellular NADPH pool to provide low-potential electron carriers (Fd, Fld, the mitochondrial iron−sulfur protein adrenodoxin) for diverse oxidoreductive metabolisms (reviewed in refs *2*, *3*).

Although there is much structural conservation within the FNR/FPR family and a common ancestor can be traced for the two-domain reductases of eukaryotes and bacteria, sequence analysis revealed the existence of two separate clusters. One is formed by all plastidic and cyanobacterial members (which are termed FNRs), and the other includes the remaining prokaryotic flavoenzymes, that constitute the FPR group (*3*). The two classes differ in the conformation of the bound FAD molecule (*7*−*9*, *19*, *20*), and in their catalytic efficiencies, with turnover numbers of 200−500 s^{-1} for *Anabaena* and chloroplast FNRs and 1−2 s^{-1} for the bacterial FPRs (*2*). These major differences in activity have been correlated with the demands of the pertinent metabolic pathways of which they are committed members (*3*). Then, bacterial FPRs have constraints on electron and/or hydride transfer that were relieved in their functional counterparts present in photosynthetic tissues and organisms, but the biochemical bases for such an improvement are unknown.

Any further understanding of the mechanisms responsible for catalytic competence in this family of flavoenzymes requires the identification of the rate-limiting step(s) in the FPR-catalyzed reactions, as already done with the reductases from plastids and cyanobacteria (*1*−*4*, *21*). To address this question, we studied the kinetics of electron and hydride transfer mediated by the FPR from the phototrophic bacterium *Rhodobacter capsulatus*, a facultative aerobe that can grow by means of fermentation, respiration, or anoxygenic photosynthesis, depending on the environmental conditions (*22*). *R. capsulatus* contains a single oxidant-responsive FPR (*18*), as well as a flavodoxin (*10*, *12*) and six different ferredoxins that could be potential substrates for this reductase (*23*, *24*). Steady-state activities measured with NADPH as reductant and Fld as electron acceptor yielded k_{cat} values of 1−2 s^{-1}, similar to those exhibited by other bacterial-type FPRs (*18*). We show here that this poor catalytic efficiency is entirely due to slow electron exchange with Fld, whereas hydride transfer to and from NADP(H) is several orders of magnitude faster. Determination of the three-dimensional structure of *R. capsulatus* FPR allowed comparison of its active site region with those of typical FNRs, to identify differences that might potentially explain the wide variation in catalytic efficiency. We have also observed that the flavin semiquinone of *Rhodobacter* Fld is remarkably stable to oxidation and a better substrate for FPR than the oxidized protein, lending support to the notion that Fld oscillates between the semiquinone and fully reduced states during turnover in vivo.

EXPERIMENTAL PROCEDURES

Protein Purification. The *Rhodobacter fpr* gene was obtained by polymerase chain reaction using chromosomal DNA from the 37b4 strain as template. The amplified fragment carrying a *Nco*I site at position −8 of the open reading frame was digested and inserted into compatible sites of the pET32a plasmid (Novagen). Recombinant FPR was obtained from cleared lysates of *Escherichia coli* BL21(DE3) transformants. Isolation by NTA (Quiagen) affinity chromatography, elution of the fusion product, enterokinase digestion, and purification of mature-sized FPR were carried out using the protocols recommended by the supplier (pET System, Novagen). The resulting protein contains two additional amino acids at the amino terminus, so that Val1 in native FPR is indicated as Val3 in the recombinant enzyme used for crystallization studies. Recombinant flavodoxin was produced and purified as described (*18*).

Photoreduction of Protein-Bound Flavin and Determination of Oxidoreduction Potentials. Photoreduction experiments were carried out at 25 °C in an anaerobic cuvette containing 15−25 μM FPR or Fld in 50 mM Tris-HCl pH 8.0, supplemented with 1 mM EDTA and 2 μM 5-deazariboflavin (dRf) to initiate flavin photoreduction via the highly reductive dRf radical (*25*). The following extinction coefficients were used for quantitative determination of redox species: FPR_{ox}, $\epsilon_{456} = 10.9$ mM^{-1} cm^{-1} (*18*); FPR_{sq}, $\epsilon_{456} = 4.4$ mM^{-1} cm^{-1} and $\epsilon_{600} = 2$ mM^{-1} cm^{-1}; FPR_{rd}, $\epsilon_{456} = 1.3$ mM^{-1} cm^{-1}; Fld_{ox}, $\epsilon_{450} = 11.7$ mM^{-1} cm^{-1} (*10*); Fld_{sq}, $\epsilon_{600} = 5.4$ mM^{-1} cm^{-1}. Extinction coefficients for Fld_{sq}, FPR_{sq}, and FPR_{rd} were determined from the spectra obtained during photoreduction of each protein, taking into account the extinction coefficient of the oxidized form and the amount of semiquinone stabilized.

Midpoint reduction potentials of *R. capsulatus* FPR and Fld were determined at 25 °C by anaerobic photoreduction in the presence of 1 μM dRf and 1 mM EDTA, using a

saturated calomel electrode as reference (*26*). Stepwise FPR or Fld photoreductions were achieved by irradiating the cell (immersed in ice water) with light from a 250 W slide projector for periods of ~1 min. After reduction, the cuvette was placed in a temperature-controlled holder in a Cary 1 spectrophotometer. The solution potential was monitored using a Sycopel Ministat potentiostat. Equilibration of the system was considered established when the measured potential remained stable for 10 min, and the UV−vis spectrum was then recorded. The concentrations of the different redox species in equilibrium were determined from the absorbance spectra. In the case of Fld, the two one-electron reductive steps could be analyzed separately because only the oxidized and semiquinone species were present during most of the first step of reduction, and only semiquinone and hydroquinone Fld were present during most of the second step. The concentration of semiquinone was calculated from the absorbance at 600 nm, and the concentrations of the other species were determined by subtraction of the semiquinone fraction from the total Fld concentration. The midpoint potentials were calculated by linear regression analysis of plots of potential versus logarithm of concentration ratio (oxidized/semiquinone or semiquinone/hydroquinone), according to the Nernst equation,

$$E = E_m + (0.059/n)\log([Flv_{ox}]/[Flv_{rd}]) \quad (3)$$

where Flv_{ox}/Flv_{rd} indicates FPR_{ox}/FPR_{rd} for the two-electron exchange in this reductase, and Fld_{ox}/Fld_{sq} or Fld_{sq}/Fld_{rd} for the two one-electron steps in Fld. Data points in the region of maximal Fld semiquinone accumulation were not included in the regression because all three redox species were present under these conditions. In the case of FPR, the semiquinone that accumulated was a small fraction of the total protein present, and only the potential of the overall two-electron reduction step ($E_{ox/rd}$) could be determined experimentally. Values for $E_{ox/sq}$ and $E_{sq/rd}$ were derived according to eqs 4 and 5, by using the measured $E_{ox/rd}$ values and the maximum molar fraction of semiquinone stabilized at half-reduction (SQ), as indicated above.

$$E_{ox/sq} - E_{sq/rd} = 0.11 \log(2\ SQ)/(1 - SQ) \quad (4)$$

$$(E_{ox/sq} + E_{sq/rd})/2 = E_{ox/rd} \quad (5)$$

The same equations were used to determine $E_{ox/rd}$ in the case of Fld. The midpoint potentials are reported relative to the potential of the standard hydrogen electrode. Typical experimental solutions contained 25−40 μM protein, 1 μM indicator dyes, 1 μM dRf, and 1 mM EDTA in 50 mM Tris-HCl pH 8.0 at 25 °C. The following dyes were used as mediators: 1 μM anthraquinone-2-sulfonate (−225 mV, pH 7) and 1 μM methyl viologen (−446 mV, pH 7) for the determination of $E_{ox/sq}$ and $E_{sq/rd}$, respectively, in Fld, and 1 μM benzyl viologen (−359 mV, pH 7) and 1 μM neutral red (−325 mV, pH 7) for the determination of $E_{ox/rd}$ in FPR. Errors in the $E_{ox/rd}$, $E_{ox/sq}$, and $E_{sq/rd}$ determinations were estimated to be ±5 mV in the case of Fld and up to ±20 mV for FPR.

Steady-State Activity of FPR. The FPR-dependent cytochrome *c* (cyt *c*) reductase activity was assayed in a Kontron Uvikon 942 or in a HP8453 diode-array spectrophotometer, using either Fld_{ox} or Fld_{sq} as electron carrier from NADPH-reduced FPR to cyt *c*. Reactions were carried out in gastight anaerobic cuvettes that contained 30 nM FPR, 50 μM cyt *c*, 1 mM glucose, and 1 unit of glucose oxidase in 800 μL of 50 mM Tris-HCl pH 8.0. Two hundred microliters of a solution made up of 17 μM Fld, 300 μM NADPH, 2 μM dRf, and 1 mM EDTA in the same buffer were added to a sidearm. The cuvette was made anaerobic by several cycles of evacuation at a vacuum pump and filling with argon. The Fld in the sidearm was either photoreduced to the semiquinone level or kept oxidized in the dark, and then tipped into the main compartment. The reduction of cyt *c* was followed by measuring the increase in absorption at 550 nm ($\epsilon_{550} = 19\ mM^{-1}\ cm^{-1}$).

Stopped-Flow Kinetic Measurements. Electron and hydride transfer processes between FPR and its substrates ($NADP^+$/NADPH or Fld) were studied by stopped-flow spectrophotometry under anaerobic conditions using an Applied Photophysics spectrophotometer interfaced with an Acorn 5000 computer and the SX.18MV software of Applied Photophysics. Reduced samples were prepared by photoreduction with dRf (*25*). The two flavoproteins were mixed at a ~1:1 molar ratio and final concentrations of ~8 μM, and electron exchange was followed at 600 nm. Hydride transfer processes with $NADP^+$/NADPH were studied by rapid mixing of ~10 μM FPR with variable concentrations (10−371 μM) of pyridine nucleotide, and the progress of the reaction was monitored at 452 nm. All assays were carried out in 50 mM Tris-HCl pH 8.0 at 25 °C. Observed rate constants (k_{obs}) were calculated by fitting the data to mono- or biexponential processes. The error in their estimated values was ±15%. Measurements of the reoxidation rates of reduced FPR and Fld by molecular O_2 were carried out in air-saturated 50 mM Tris-HCl pH 8.0.

Crystallization and Data Collection. The strategy followed to obtain suitable FPR crystals has been reported elsewhere (*27*). Briefly, FPR from *R. capsulatus* was crystallized in two different forms consisting of trigonal and monoclinic crystals. Trials were carried out by the hanging drop vapor diffusion method at 291 K, and drops were equilibrated against 500 μL of a well solution made up of 2 M ammonium sulfate and 2% (v/v) 2-propanol buffered with 0.1 M Bis-Tris pH 6.5. Monoclinic crystals grew in 4-μL droplets formed by mixing 2 μL of a 6.9 mg/mL protein solution in 50 mM Tris-HCl pH 8.0 with 2 μL of the well solution. Crystals reached their maximum size of 0.7 × 0.3 × 0.3 mm in 1−2 days. Trigonal crystals were obtained under the same conditions but in the presence of the detergent *n*-heptyl-β-D-thioglucoside (HTG). They grew in 10-μL droplets formed by mixing 4 μL of a 25.5 mg/mL protein solution in 50 mM Tris-HCl pH 8.0 with 1 μL of 300 mM HTG and 5 μL of well solution. Crystals reached their maximum size of 1.6 × 0.3 × 0.3 mm in 1−2 days.

An X-ray data set for trigonal crystals was collected up to 1.7 Å resolution using the synchrotron radiation source at ESRF (Grenoble) on beamline ID14-2 ($\lambda = 0.934$ Å) and an ADSC Q4 detector. They belong to the $P3_121$ space group and have unit cell dimensions of $a = b = 120.85$ Å, $c = 50.71$ Å, $\alpha = \beta = 90°$, $\gamma = 120°$. The V_M is 3.56 $Å^3\ Da^{-1}$ with one molecule in the asymmetric unit and a solvent content of 64%. X-ray data for monoclinic crystals were obtained up to 2.1 Å resolution on a MAR345 image-plate

Table 1: Structure Determination and Statistics for Trigonal and Monoclinic FPR Crystals[a]

	trigonal	monoclinic
Data Collection Statistics		
space group	$P3_121$	$P2_1$
unit cell parameters		
a, Å	120.85	69.23
b, Å	120.85	93.63
c, Å	50.71	103.43
α, deg	90.0	90.0
β, deg	90.0	90.08
γ, deg	120.0	90.0
no. of molecules/au	1	4
wavelength, Å	0.9340	1.5418
resolution, Å	45.6−1.7 (1.8−1.7)	22.8−2.1 (2.3−2.1)
total no. of reflections	1112404	590176
no. of unique reflections	61984	73447
redundancy	7.3 (7.5)	3 (2.6)
completeness, %	97.2 (90.0)	99.0 (60.4)
I/σ	11.2 (2.6)	10.3 (2.3)
R_{merge}[b]	0.117 (0.649)	0.079 (0.369)
Refinement Statistics		
resolution range, Å	45.6−1.7	22.8−2.1
non-hydrogen atoms		
protein	2031	8148
ligand	121	212
solvent	265	362
R_{work}	0.22	0.22
R_{free}[c]	0.23	0.24
rmsd bond length, Å	0.007	0.013
rmsd bond angles, deg	1.572	1.353
average *B*-factor, Å^2	43.24	42.15

[a] Values in parentheses correspond to the highest resolution shell. [b] $R_{sym} = \Sigma|I - I_{av}|/\Sigma I$, where the summatory is over symmetry equivalent reflections. [c] *R* calculated for 7% of data excluded from the refinement.

detector using graphite monochromatic Cu Kα ($\lambda = 1.5418$ Å) radiation generated by an Enraf-Nonius rotating anode generator. These crystals belong to the $P2_1$ space group with unit cell dimensions of $a = 69.23$ Å, $b = 93.63$ Å, $c = 103.43$ Å, $\alpha = \gamma = 90°$, $\beta = 90.08°$. The V_M is 2.8 Å^3 Da^{-1} with four FPR molecules in the asymmetric unit and a solvent content of 56%. Data were processed and scaled using the programs MOSFLM (*28*) and SCALA from the CCP4 package (*29*). In all cases, crystals were cryoprotected by a quick soak (10 s) in reservoir solution containing 50% saturated sodium formate. Data collection statistics are given in Table 1.

Structure Determination and Refinement. The native structures of both trigonal and monoclinic crystal forms were determined by the molecular replacement method using the program AMoRe (*30*). In the trigonal case, the initial model employed was the structure of FPR from *Azotobacter vinelandii*, which displays 53% sequence identity with the *Rhodobacter* reductase. In the monoclinic crystals, the molecular replacement method was used on the basis of the FPR model obtained from the trigonal crystals. Unambiguous single solutions for the rotation and translation functions were obtained in both cases. The models were subjected to alternate cycles of refinement with the program CNS (*31*), and manual model building with the software package O (*32*). The resulting electron density was of great quality for 257 or 260 residues out of a total of 272 amino acids for the trigonal and monoclinic forms, respectively. The quality of the final structure was assessed with the PROCHECK (*33*) and WHATCHECK (*34*) programs. Statistics for refinement are summarized in Table 1. The final FPR model obtained in the presence of detergent (trigonal form) consists of 2031 non-hydrogen protein atoms, one FAD and three HTG molecules, one sulfate and two formate anions, and 265 solvent molecules. The final FPR model obtained in the absence of detergent (monoclinic form) consists of 8148 non-hydrogen protein atoms (four molecules per asymmetric unit), four FAD molecules, and 362 solvent molecules. Pictures were generated with MOLSCRIPT (*35*) and GRASP (*36*).

RESULTS

Three-Dimensional Structure of R. capsulatus FPR. The crystal structure of FPR was solved in two different crystal forms obtained in the presence or in the absence of the detergent HTG (Table 1). The two structures were refined up to 1.7 and 2.1 Å resolution, respectively, showing similar conformations with a root-mean-square deviation (rmsd) of 0.75 Å for 257 Cα atoms, the main differences being concentrated in exposed regions displaying a large number of hydrophobic residues (Figure 1A). FPR is composed of two domains, an N-terminal region (residues 12 to 110 of the recombinant protein) that binds FAD and a C-terminal domain (residues 111−272) that interacts with $NADP^+$/NADPH (Figure 1). The N-terminal domain contains a six-stranded all antiparallel *β*-barrel with a capping α-helix (α1, residues 87−96). FAD is bound at the crossover between strands *β*4 and *β*5, and at the N-terminal end of the α1 helix (Figure 1A). The C-terminal domain represents a classical nucleotide binding fold with a five-stranded parallel *β*-sheet, and nine helices (α2−α10) inserted between the *β*-strands (Figure 1A). By comparison with known structures from the FNR/FPR family, the $NADP^+$ binding site extends across the C-terminal ends of the *β*-strands of the parallel sheet, so that the FAD and $NADP^+$ sites are adjacent in a deep cleft formed between the two domains. Detergent-binding sites for HTG1 and HTG2 define a hydrophobic region formed by residues 142−147, residues 177−182, and Trp73 (Figure 1A). The other detergent molecule, HTG3, only makes crystal packing contacts through nonspecific interactions with two symmetry-related FPR molecules.

A search for structural similarities (*37*) with the complete FPR structure shows that, besides from *A. vinelandii* FPR (rmsd of 1.2 Å for 253 Cα atoms), the closest relatives are the FPR from *E. coli* (rmsd of 1.8 Å for 239 Cα atoms) and benzoate 1,2-dioxygenase reductase from *Acinetobacter* sp. (rmsd of 2.4 Å for 219 Cα atoms). As anticipated, the plastidic and cyanobacterial members of the FNR/FPR family show greater differences (rmsd of 2.9 Å for 224 Cα atoms of *Anabaena* FNR).

The conformation of FAD and its binding site are shown in Figure 1B. As in other bacterial FPRs (*19*, *20*), the prosthetic group adopts a bent conformation, with the AMP portion folded back and placing the adenine and isoalloxazine rings in proximity, whereas in plant and *Anabaena* FNRs the cofactor is extended so that the adenine is distal from the isoalloxazine ring system (*7*−*9*). In *R. capsulatus* FPR, the adenine is sandwiched between Ile82 and Phe267 (Figure 1B), while in plastidic FNRs, it is oriented toward the solvent by stacking stabilization with a tyrosine (Tyr104 in *Anabaena* FNR), which is placed in a long and flexible loop corre-

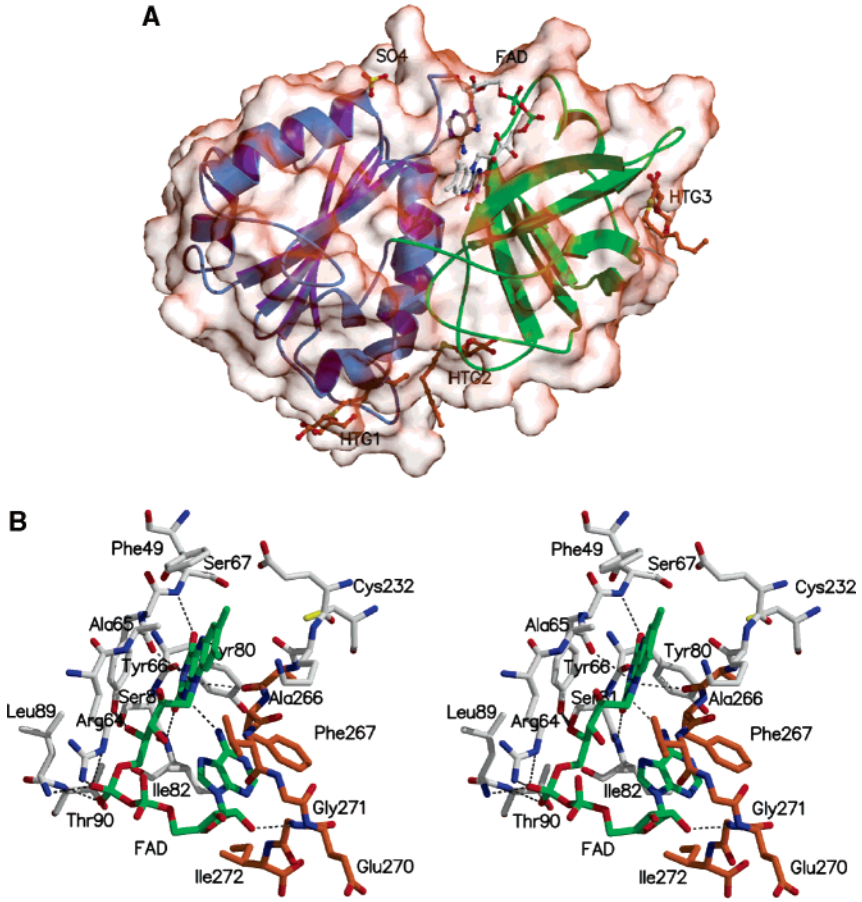

FIGURE 1: Overall structure of *R. capsulatus* FPR. (A) Ribbon diagram of FPR, with the binding domains for FAD and $NADP^+$ colored in green and magenta, respectively. The FAD prosthetic group, the sulfate anion, and the three HTG molecules are represented as balls and sticks. (B) Stereodiagram of the residues lining the FAD binding site, shown in ball-and-stick representation, and colored by atom type. The C-terminal region comprising residues 266−272 is colored in orange and the FAD cofactor in green. The polar network involved in FAD stabilization is represented as dotted lines.

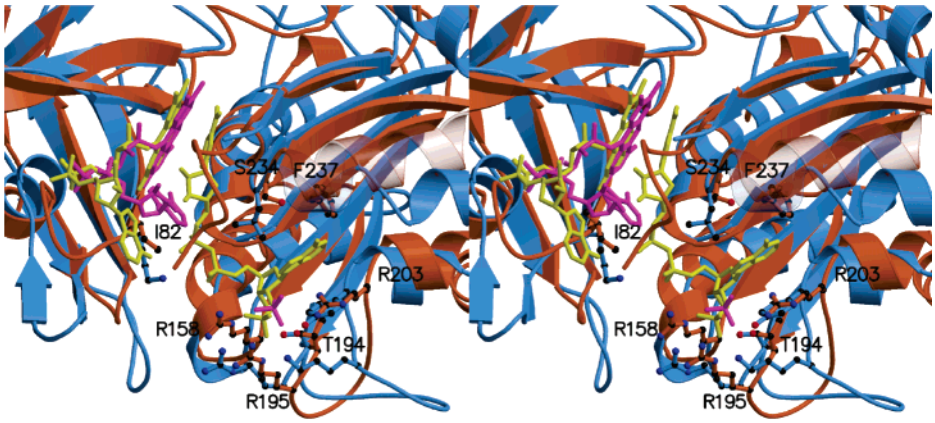

FIGURE 2: The $NADP^+$ binding region of *R. capsulatus* FPR. Stereoview of free FPR (orange) and mutated pea FNR with bound $NADP^+$ (blue), superimposed by the least-squares fitting of the whole FNR/FPR structure. FAD and $NADP^+$ in the complex are colored in yellow, while FAD in the free enzyme and the sulfate ion found in the FPR structure are colored in magenta. Residues presumably involved in coenzyme binding are represented as balls and sticks and colored in blue for the FNR:$NADP^+$ complex and in orange for free FPR.

sponding to residues 102−116 (*38*). This loop is very short in *R. capsulatus* FPR, comprising only amino acids 84−88, and its flexibility is further compromised by the presence of two prolines and no aromatic residues (Figure 2). The isoalloxazine moiety lacks the stacking interaction between its *re*-face and a C-terminal aromatic residue as observed in plastidic FNRs or *E. coli* FPR. On the other side of the flavin, the conserved Tyr66 does interact with the *si*-face of FAD at an angle of about 30° (Figure 1B).

The 6-residue C-terminal extension (amino acids 267−272) is especially important in the stabilization of the FAD cofactor (see Figure 1B). As indicated above, Phe267 stabilizes the adenine portion of the FAD. In addition to this aromatic contact, Val268 and Gly271 are engaged in polar interactions with the ribitol and ribose rings of the FAD through their amide groups. Folding of the C-terminal region over the prosthetic group is additionally supported by hydrogen bonds between the amide groups of Leu235,

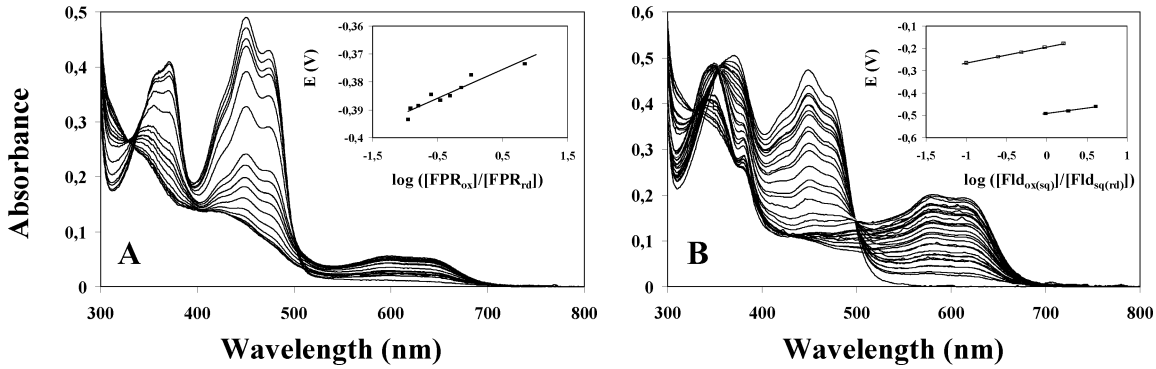

FIGURE 3: Photoreduction of the *R. capsulatus* FPR (A) and Fld (B) flavins. The flavoproteins were photoreduced by dRf in 50 mM Tris-HCl pH 8.0 at 25 °C, as indicated under Experimental Procedures, and spectra were recorded at 1-min intervals. The insets show the corresponding Nernst plots.

Phe267, and Gly269 and a water molecule (Figure 2A). Interestingly, the C-terminal residue, Ile272, is stabilized through a hydrogen bond with the amide group of Arg158.

Figure 2 displays the FPR structure superimposed to the C-terminal Y308S mutant of pea FNR in complex with $NADP^+$ (*39*), highlighting both the region to which $NADP^+$ binds and the residues involved in molecular recognition. The overall conformation of the $NADP^+$ binding domain is well conserved between the two enzymes, although important structural differences are observed in the 233−235 loop and the α7 helix, and in the 193−204 stretch connecting β9 with the α6 segment (Figure 2).

Structural rearrangements in the active site of plastidic FNR have been observed upon $NADP^+$ binding (*38*, *39*), and postulated to be part of a general mechanism of molecular recognition and complex reorganization necessary for hydride transfer between FNR and $NADP^+$ (*38*). Comparison with the mutated pea FNR:$NADP^+$ complex reveals significant differences in the amino acids present at the $NADP^+$ binding site of FPR, most conspicuously, the lack of an aromatic side chain at position 203 (Figure 2). A Tyr residue is always present in the corresponding position of plastidic FNRs, allowing both a stacking interaction with the adenine ring and a polar contact with the 2′-phosphate. In contrast, Arg203 of *Rhodobacter* FPR interacts with a sulfate anion placed at a position equivalent to that of the 2′-phosphate in bound $NADP^+$ (Figure 2). Interestingly, a stabilizing contact could be established between the amide group of arginine and the adenine ring of the pyridine nucleotide (cation−π interaction).

Oxidoreductive Properties of R. capsulatus FPR and Fld. Photoreduction of FPR and Fld under anaerobic conditions allowed estimation of the maximal amount of neutral flavin semiquinone stabilized during reduction. FPR displayed anomalous photoreduction behavior, often exhibiting partial reoxidation relative to the previous cycle between successive illumination rounds. Since measurements were carried out under a range of conditions with different samples, and since O_2 was rigorously excluded from the system, the observed effect must be due to an intrinsic property of this FPR. However, we cannot yet explain the phenomenon. The measurements of the percentage stabilization of the semiquinone and of the redox potentials were made after this period of partial reoxidation. Data derived from the spectra of Figure 3A indicate that FPR accumulated a maximum of 30% of the total FAD as semiquinone, in close agreement with the percentages reported for *Anabaena* FNR (*1*, *4*). In contrast, photoreduction of Fld followed a normal pattern and its semiquinone form reached up to 96% of the total FMN present in the bacterial electron carrier (Figure 3B). Exposure of the fully reduced flavoproteins to air led to complete oxidation of FPR in a few seconds, whereas Fld was only oxidized to the semiquinone state, and thereafter remained stable for several hours (data not shown).

Table 2: Midpoint Reduction Potentials of *R. capsulatus* FPR and Fld[a]

flavoprotein	$E_{ox/rd}$ (mV)	$E_{ox/sq}$ (mV)	$E_{sq/rd}$ (mV)	% SQ
FPR	−381	−384[b]	−377[b]	30
Fld	−343[b]	−200	−487	96[b]

[a] Experiments were carried out in 50 mM Tris-HCl, pH 8.0 at 25 °C. [b] These values were calculated using eqs 4 and 5 as described in the text.

The redox potential for the two-electron reduction of FPR ($E_{ox/rd}$) was determined experimentally to be −381 mV. The FPR potentials for the one-electron exchanges, calculated according to eqs 4 and 5 and using the reported $E_{ox/rd}$ and maximal semiquinone fractions, were $E_{ox/sq} = -384$ mV and $E_{sq/rd} = -377$ mV (Table 2). These values are in the range of those reported for FNRs from different sources, such as the *Anabaena* ($E_{ox/rd} = -374$ mV, ref *40*) and spinach reductases ($E_{ox/rd} = -380$ mV, ref *41*), despite differences in the buffer composition, temperature, or pH.

The two one-electron potentials of Fld could be measured experimentally because the semiquinone is very stable. The values determined were −200 mV for $E_{ox/sq}$ and −487 mV for $E_{sq/rd}$, while that calculated for $E_{ox/rd}$ was −343 mV (Table 2). These results are in full agreement with those reported by Hallenbeck and Gennaro (*42*).

Fast Kinetic Studies of Hydride Exchange between FPR and NADP(H). Reaction of the oxidized reductase with NADPH was studied using stopped-flow methods, by following the decrease in flavin absorption at 452 nm under anaerobic conditions. Transients were best fit by monoexponential curves whose observed rate constants (k_{obs}) increased with nucleotide concentration (Figure 4A). Similar results were obtained when photoreduced FPR was rapidly mixed with $NADP^+$ and the reactions were followed by the increase in absorption at 452 nm (Figure 5A), although in this case somewhat lower rates were observed. For both processes, the k_{obs} values approached maxima as the nucleotide concentration was raised (Figures 4B and 5B), allowing

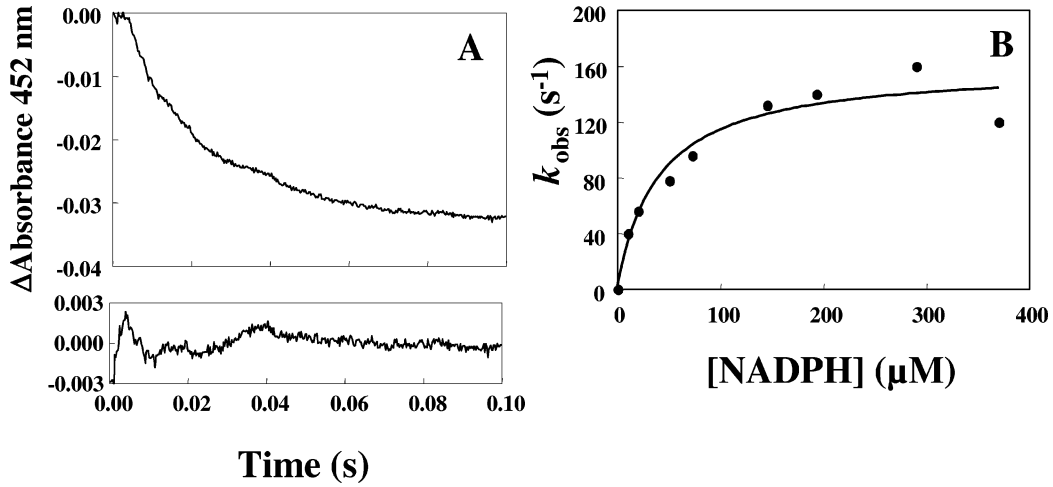

FIGURE 4: Time course of anaerobic reduction of *R. capsulatus* FPR_{ox} by NADPH. (A) FPR_{ox} (~10 μM) was mixed with NADPH (20 μM, final concentration). The residual for this fitting is shown at the bottom. (B) Dependence of the observed rate constants for FNR_{ox} reduction on NADPH concentration. Reactions were carried out in 50 mM Tris-HCl, pH 8.0 at 25 °C.

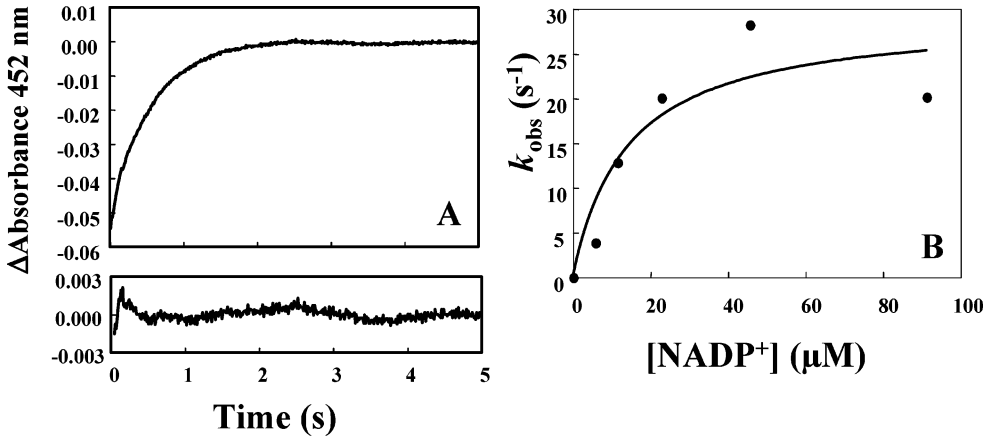

FIGURE 5: Time course of anaerobic reduction of $NADP^+$ by *R. capsulatus* FPR_{rd}. (A) Photoreduced FPR_{rd} (~10 μM) was mixed with $NADP^+$ (12 μM, final concentration). The residual for this fitting is shown at the bottom. (B) Dependence of the apparent rate constants for FPR_{rd} oxidation on $NADP^+$ concentration. Reactions were carried out in 50 mM Tris-HCl, pH 8.0 at 25 °C.

Table 3: Steady-State and Single Turnover Parameters of *R. capsulatus* FPR with NADP(H) and Fld

reaction	K_d (μM)	k_{et} (s^{-1})	k_{obs1} (s^{-1})	k_{obs2} (s^{-1})	k_{ap} (s^{-1})
Hydride Transfer					
from NADPH to FPR_{ox}	60	150			
from FPR_{rd} to $NADP^+$	20	30			
Electron Transfer					
from Fld_{rd} to FPR_{ox}			9.3	1.5	
from FPR_{rd} to Fld_{ox}			2.7	1.0	
from FPR_{rd} to Fld_{sq}			18.8	1.6	
Cytochrome *c* Reductase Activity					
with *Rhodobacter*					
Fld_{ox}					0.26
Fld_{sq}					0.85
with *Anabaena*					
Fld_{ox}					1.50
Fld_{sq}					4.09

calculation of the dissociation constants (K_d) for the intermediate FPR_{ox}/NADPH and FPR_{rd}/$NADP^+$ complexes (Table 3). The absolute rates of hydride transfer (k_{et}), reached at saturating substrate concentration, were 150 s^{-1} and 30 s^{-1} for NADPH oxidation and $NADP^+$ reduction, respectively (Figures 4 and 5, Table 3). Thus, the physiological direction of hydride transfer is more rapid than the backward reaction, although both processes occur at least 1 order of magnitude faster than steady-state turnover (*18*), and neither of them represents the rate-limiting step in FPR catalysis.

Electron Exchange Reactions between FPR and Fld. Stopped-flow kinetic studies were carried out to further investigate the time course of association and electron transfer between FPR and Fld in the two possible directions (*25*). Formation of the semiquinone forms in both flavoproteins was monitored by following the absorption changes at 600 nm (Figure 6). Two phases with k_{obs} of about 9 s^{-1} and 1.5 s^{-1} could be detected during reduction of the oxidized reductase by Fld_{rd} (Figure 6A and Table 3), probably reflecting two successive electron transfer reactions (*25*). The initial increase in absorbance at 600 nm indicates that reaction of FPR_{ox} with Fld_{rd} led to the formation of both semiquinones by a single electron transfer from Fld_{rd} to FPR_{ox}. However, this increase was shortly followed by a decline in absorbance at a slower rate. Taking into account that the semiquinone state of Fld is highly stable (Figure 3B), it is noteworthy that the relatively small amount of semiquinone stabilized at the end of the process. Such an observation is consistent with a mechanism in which the Fld_{sq} resulting from the initial electron transfer from Fld_{rd} to FPR_{ox} reacts either by electron exchange with FPR_{sq} or by disproportionation. However,

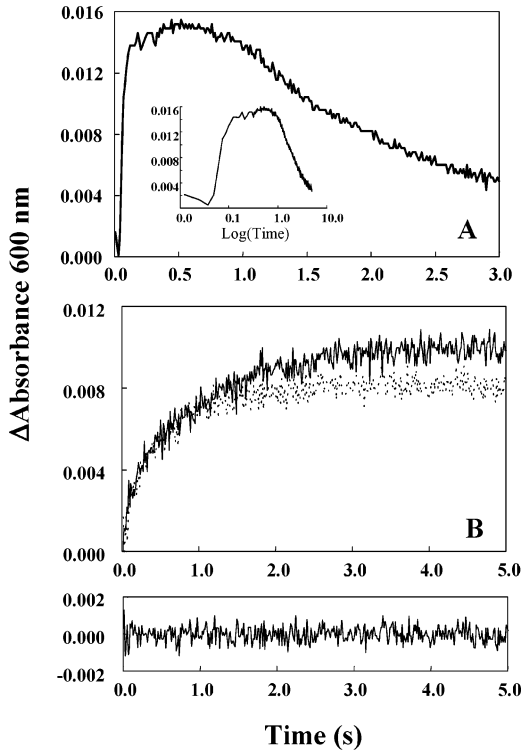

FIGURE 6: Kinetics of electron exchange between *R. capsulatus* FPR and Fld. (A) Time course of the anaerobic reaction of Fld_{rd} with FPR_{ox}. The inset shows the same kinetics in logarithmic time representation. (B) Time course of the anaerobic reactions of FPR_{rd} with Fld_{ox} (dotted line; the residual for this fitting to a biexponential process is shown at the bottom) and of FPR_{rd} with Fld_{sq} (solid line). The two proteins were mixed at a 1:1 ratio and final concentrations of ~8 μM. Reactions were carried out in 50 mM Tris-HCl, pH 8.0 at 25 °C.

further analysis of the fast kinetic intermediate species at different wavelengths will be required in order to unequivocally identify the nature of this reaction.

The reverse reaction also displayed biphasic kinetics but with lower rates (Figure 6B and Table 3). Thus, the latter process appears to be slow enough to be the rate-limiting step of the physiological FPR reaction in *Rhodobacter*, namely, electron transfer from NADPH to the oxidized protein substrate.

Since the semiquinone state of *R. capsulatus* Fld proved to be so stable to oxidation, it was possible to assay the ability of this form to act as electron donor and acceptor with oxidized and reduced FPR, respectively. The reaction could be followed at 452 and 600 nm, to detect changes in the fully oxidized and semiquinone species of the two flavin-containing redox partners. Rapid mixing of Fld_{sq} and FPR_{ox} under anaerobic conditions failed to show perturbations in the absorbance at the two wavelengths (data not shown), suggesting that no reaction occurred between these species. In contrast, FPR_{rd} reduced Fld_{sq} at a relatively high rate (k_{obs} = 19 s^{-1}, Figure 6B and Table 3), indicating that the semiquinone form of Fld is a better acceptor than Fld_{ox} for FPR. A second, much slower process, with k_{obs} = 1.6 s^{-1}, was also detected. Such a process might be related to electron transfer reactions between residual Fld_{ox} and Fld_{rd} species present in equilibrium with the reacting Fld_{sq} and the different redox states of FPR present during the overall process.

These results raised the possibility that, during steady-state turnover from NADPH to Fld, reduction of the acceptor to the semiquinone level could limit the rate of the overall reaction. This possibility was tested, taking advantage of the high redox stability of Fld_{sq}. FPR activity is routinely measured in vitro by a coupled assay with cyt *c*, a final acceptor that competes favorably with oxygen for the available electron of reduced Fd or Fld (*18*). When the reactions were carried out in the absence of oxygen, the initial rates of cyt *c* reduction increased from 0.26 s^{-1} for Fld_{ox} to 0.85 s^{-1} for Fld_{sq}. This increase presumably indicates that under these conditions Fld_{ox} is not re-formed in the first catalytic cycle and that Fld_{sq} is the substrate in subsequent rounds (Table 3). Similar effects were observed with *Anabaena* Fld and FNR (Table 3). During steady-state catalysis, Fld_{sq} will be reduced to the hydroquinone state by reduced FPR, and reoxidized back to the semiquinone by either cyt *c* or oxygen. If the reaction is carried out with Fld in its oxidized form, a one-electron reduction to the semiquinone must first occur before the more rapid redox cycle between semiquinone and hydroquinone can begin. Given the high redox stability of *Rhodobacter* Fld_{sq}, it was not necessary to use anaerobic conditions for the cyt *c* reductase assay. Oxygen was excluded in order to compare the results with those obtained with the *Anabaena* Fld, which is rapidly oxidized in air.

DISCUSSION

The first detailed description of the kinetic mechanism of a ferredoxin-NADP(H) reductase was based on substrate binding assays, rapid mixing experiments, and steady-state measurements carried out on spinach FNR (*21*). $NADP^+$ reduction (the direction most relevant for photosynthetic organisms) follows a compulsory ordered mechanism with the nucleotide acting as the leading substrate, whereas the backward reaction proceeds via a two-step transfer mechanism without formation of a ternary complex (*2* and references therein). In this case, NADPH also binds first to the enzyme, but $NADP^+$ is expected to dissociate before Fd or Fld binding. The overall reactions involve several individual steps including hydride and electron exchange, as well as substrate binding and product release from various FNR forms. In the forward photosynthetic direction leading to NADPH synthesis, dissociation of the oxidized Fd product has been identified as rate limiting for catalysis by chloroplast FNR (*21*). Our knowledge on the mechanisms underlying NADPH oxidation mediated by either heterotrophic FNRs or bacterial FPRs lags way behind, but the accumulated evidence suggests that the entire reaction is restricted by processes involving Fd or Fld (*2*).

Taking into account the high degree of structural conservation in the FNR/FPR family, it is surprising that the photosynthetic and bacterial reductases display such different turnover rates. The low k_{cat} values of prokaryotic FPRs could be caused, in principle, by constraints imposed on one or more of the various binding/dissociation and redox processes. Previous studies have shown that affinity results for $NADP^+$, Fd_{ox}, or Fld_{ox} were in the same micromolar range for typical members of the FNR and FPR classes (*1*, *2*, *4*, *18*, *43*, *44*). In the present article, we have observed that electron transfer from reduced FPR to oxidized Fld is the slowest step during enzyme turnover, taking place at about 2.7 s^{-1} (Table 3). Identification of Fld_{ox} reduction as rate limiting for FPR catalysis in vitro does not exclude the possibility that other

individual steps, such as dissociation of the enzyme:$NADP^+$ complex, could also constrain steady-state activity. However, two observations argue against this possibility. First, $NADP^+$ interaction with reduced FPR was found to be rather weak, with a $K_d = 20\ \mu M$, as revealed by stopped-flow measurements (Figure 5 and Table 3). More importantly, replacement of Fld_{ox} by Fld_{sq} resulted in a significant increase of electron transfer rates under both single turnover and steady-state conditions (Table 3), indicating that Fld_{ox} reduction was indeed the limiting step for catalysis.

To the best of our knowledge, the results presented here provide the first kinetic evidence showing that, at least in *Rhodobacter*, Fld_{sq} is the preferred substrate for FPR. The nature of the redox transitions taking place during function of this flavoprotein in vivo has been a matter of controversy for years. Much of the discussion has concentrated on the turnover of FMN in the "Fld-like" domains of diflavin reductases, an important family of enzymes containing built-in Fld and FNR/FPR units that includes cytochrome P450 reductase (P450R), nitric oxide synthase, and sulfite reductase, among others (*45*). These enzymes mediate hydride transfer from NADPH to FAD, followed by intramolecular electron transfer to FMN, and from it to the final acceptor (*45*−*47*). The inability of the air-stable FMN semiquinone of P450R (*48*) and nitric oxide synthase (*47*) to reduce cytochrome *c* and adriamycin, respectively, has been regarded as a proof indicating that the fully reduced flavin must be the necessary electron donor, but this evidence has been challenged on the argument that the air-stable neutral semiquinone was not part of the catalytic cycle (*45*). Instead, the anionic form of the FMN semiquinone was proposed to be the catalytically relevant intermediate in the *Bacillus megaterium* P450R (*46*).

The electron transfer system established by "free-living" FPR and Fld represents a split version of diflavin reductases, and has been shown to catalyze P450R activity, albeit with lower efficiency (*43*, *49*, *50*). Important differences in the reduction potentials could account, at least in part, for the wide variation in specific activity observed among the various systems (*43*, *45*−*47*). Of the two possible redox transitions that free Fld can undergo, the one involving the semiquinone and hydroquinone forms has a midpoint potential similar to that of the Fe^{3+}/Fe^{2+} transition of isofunctional Fd in many species, whereas $E_{ox/sq}$ values are less negative (Table 2, see also ref *42*). Based on these considerations, it has been argued that Fld may swing between the semireduced and fully reduced forms during turnover in vivo (*51*), although on purely thermodynamic grounds, Fld_{ox} should be a better oxidant for FPR_{rd} during electron transfer from NADPH to the protein partner (*43*). It is worth noting that this reaction, occurring in heterotrophic tissues and organisms, represents the most extended function of the FPR/FNR enzymes in nature (*2*, *3*). Bacteria thriving on anoxygenic photosynthesis, including *Rhodobacter*, also use FPR activity to reduce low-potential electron carriers such as Fld via NADPH oxidation (*18*). In this context, the low $E_{sq/rd}$ value of *Rhodobacter* Fld (Table 2) supports the notion that this flavoprotein could be part of a physiological electron path to the nitrogenase, and might transfer reducing equivalents to the iron−sulfur protein component of that complex, which displays a midpoint potential of about −440 mV (*42*). The two proteins bind tightly in solution ($K_d = 0.44\ \mu M$) and rapid electron transfer occurs in the presence of dithionite, whereas Fd was found to be a very inefficient donor (*42*).

Table 4: Amino Acid Residues Conserved in *R. capsulatus* FPR and *Anabaena* FNR

Rhodobacter FPR	*Anabaena* FNR
Arg64	Arg77
Ala65	Leu78
Tyr66	Tyr79
Ser67	Ser80
Cys232	Cys261
Glu264	Glu301

Our results thus show that the advantages of Fld_{ox} as electron acceptor are frustrated by kinetic restrictions that severely hamper this thermodynamically favored reaction. There are many examples of flavin-mediated reactions that proceed against the reduction potential, as recently reviewed by Murataliev et al. (*45*). The question remains open as to which molecular traits might be held responsible for the suboptimal reaction rates of the bacterial FPR class. Comparison of the active site region of *R. capsulatus* FPR with those of typical FNR prototypes reveals many distinct features (Figures 1 and 2). Some of them occur at the nucleotide binding pocket of the bacterial reductase (Figure 2), including the absence of aromatic stacking on the flavin that allows discrimination between NADP(H) and NAD(H) in the plant reductases, the lack of a positive charge stabilizing the pyrophosphate group, the distinct conformation of Tyr66 on the *si*-side of the flavin, and the entirely different architecture of the hydrogen bond network of the site (Figures 1 and 2). While these changes most certainly determine a distinct set of interactions during NADP(H) binding and orientation in FPR relative to FNR, the results displayed in Table 3 indicate that they do not limit hydride transfer or FPR catalysis.

The role(s) played by amino acids at the active site during binding and reaction with Fld (the actual rate-limiting step of FPR turnover) are even less understood. Protein−protein interaction is likely governed by a combination of electrostatic and hydrophobic forces, as proposed for the FNRs involved in oxygenic photosynthesis (*1*, *4*). The orientation of the FPR dipole moment is similar to that of FNR, with values of 533 and 710 D for the *Rhodobacter* and *Anabaena* reductases, respectively, as calculated by using GRASP (data not shown). Moreover, a number of basic residues, including Arg43, Lys60, Arg105, Lys107, and Lys265, form a crown in the FAD-binding domain of FPR at the putative binding site for the protein partners, and might be involved in steering the initial encounter, while other forces could participate in achieving the optimal orientation of the components in the complex competent for electron transfer.

In addition to the amino acids interacting with the substrates, several other residues implicated in the catalytic mechanism of FNR (Tyr79, Ser80, Cys261, and Glu301 in the *Anabaena* reductase) are conserved in FPR (Tyr66, Ser67, Cys232, and Glu264; see Table 4 and Figure 1B). Therefore, a similar function could be expected for these amino acids in the two enzyme types. With respect to the contribution of the nonconserved C-terminal tyrosine to electron transfer in FNR, Nogués et al. (*40*) have recently shown that this residue is not involved in the electron shuttling pathway between the prosthetic groups. Instead, it favors stabilization

of the flavin semiquinone form required for electron splitting, and modulates the rates of electron exchange with Fd and Fld (*40*). It is conceivable that the different architecture of the C-terminal region of FPR may have critical effects on these activities, but experimental support for this contention remains yet to be established.

The collected results suggest that the initial complex formed between *R. capsulatus* FPR and Fld, dominated by electrostatic interactions, is probably similar to that of its FNR siblings. The low rates of electron exchange between FPR and Fld are also not caused by major shifts in the redox potentials of the flavoproteins that might thwart their reaction. More likely, they reflect imperfect orientation of the prosthetic groups in the functional complex, and/or impaired electron convection between the redox partners. The crystal structure of the bacterial FPR reveals differential conformations and nonconserved residues that might explain its low catalytic competence, but a thorough identification of these mechanistic determinants will require the use of directed mutagenesis and the obtention of FPR−Fld complexes amenable to X-ray crystallography to identify those residues and interactions that were modified in the course of evolution to accomplish the formidable increase in catalytic efficiency that led to the FNR versions of the family.

REFERENCES

1. Hurley, J. K., Morales, R., Martinez-Júlvez, M., Brodie, T. B., Medina, M., Gómez-Moreno, C., and Tollin, G. (2002) Structure−function relationships in *Anabaena* ferredoxin/ferredoxin:$NADP^+$ reductase electron transfer: insights from site-directed mutagenesis, transient absorption spectroscopy and X-ray crystallography, *Biochim. Biophys. Acta 1554*, 5−21.
2. Carrillo, N., and Ceccarelli, E. A. (2003) Open questions in ferredoxin-NADP(H) reductase catalytic mechanism, *Eur. J. Biochem. 270*, 1900−1915.
3. Ceccarelli, E. A., Arakaki, A. K., Cortez, N., and Carrillo, N. (2004) Functional plasticity and catalytic efficiency in plant and bacterial ferredoxin-NADP(H) reductases, *Biochim. Biophys. Acta 1698*, 155−165.
4. Medina, M., and Gómez-Moreno, C. (2004) Interaction of ferredoxin-$NADP^+$ reductase with its substrates: optimal interaction for efficient electron transfer, *Photosynth. Res. 7*9, 113−131.
5. Karplus, P. A., and Faber, H. R. (2004) Structural aspects of plant ferredoxin:$NADP^+$ oxidoreductases, *Photosynth. Res. 81*, 303−315.
6. Hanke, G. T., Kurisu, G., Kusunoki, M., and Hase, T. (2004) Fd: FNR electron transfer complexes: evolutionary refinement of structural interactions, *Photosynth. Res. 81*, 317−327.
7. Karplus, P. A., Daniels, M. J., and Herriott, J. R. (1991) Atomic structure of ferredoxin-$NADP^+$ reductase: prototype for a structurally novel flavoenzyme family, *Science 251*, 60−66.
8. Bruns, C. M., and Karplus, P. A. (1995) Refined crystal structure of spinach ferredoxin-$NADP^+$ oxidoreductase at 1.7 Å resolution: oxidized, reduced and 2′-phospho-5′-AMP bound states, *J. Mol. Biol. 247*, 125−145.
9. Serre, L., Vellieux, F. M., Medina, M., Gómez-Moreno, C., Fontecilla-Camps, J. C., and Frey, M. (1996) X-ray structure of the ferredoxin-$NADP^+$ reductase from the cyanobacterium *Anabaena* PCC7119 at 1.8 Å resolution, and crystallographic studies of $NADP^+$ binding at 2.25 Å resolution, *J. Mol. Biol. 263*, 20−39.
10. Yakunin, A. F., Gennaro, G., and Hallenbeck, P. C. (1993) Purification and properties of a *nif*-specific flavodoxin from the photosynthetic bacterium *Rhodobacter capsulatus*, *J. Bacteriol. 175*, 6775−6780.
11. Razquin, P., Fillat, M. F., Schmitz, S., Stricker, O., Bohme, H., Gómez-Moreno, C., and Peleato, M. L. (1996) Expression of ferredoxin-$NADP^+$ reductase in heterocysts from *Anabaena* sp., *Biochem. J. 316*, 157−160.
12. Gennaro, G., Hubner, P., Sandmeier, U., Yakunin, A. F., and Hallenbeck, P. C. (1996) Cloning, characterization, and regulation of *nifF* from *Rhodobacter capsulatus*, *J. Bacteriol. 178*, 3949−3952.
13. Erdner, D. L., Price, N. M., Doucette, G. J., Peleato, M. L., and Anderson, D. M. (1999) Characterization of ferredoxin and flavodoxin as markers of iron limitation in marine phytoplankton, *Mar. Ecol.: Prog. Ser. 184*, 43−53.
14. Yousef, N., Pistorius, E. K., and Michel, K. P. (2003) Comparative analysis of *idiA* and *isiA* transcription under iron starvation and oxidative stress in *Synechococcus elongatus* PCC 7942 wild-type and selected mutants, *Arch. Microbiol. 180*, 471−483.
15. Singh, A. K., Li, H., and Sherman, L. A. (2004) Microarray analysis and redox control of gene expression in the cyanobacterium *Synechocystis* PCC 6803, *Physiol. Plant. 120*, 27−35.
16. Zheng, M., Doan, B., Schneider, T. D., and Storz, G. (1999) *OxyR* and *SoxRS* regulation of *fur*, *J. Bacteriol. 181*, 4639−4643.
17. Krapp, A. R., Rodríguez, R. E., Poli, H. O., Paladini, D. H., Palatnik, J. F., and Carrillo, N. (2002) The flavoenzyme ferredoxin(flavodoxin)-NADP(H) reductase modulates NADP(H) homeostasis during the *soxRS* response of *Escherichia coli*, *J. Bacteriol. 184*, 1474−1480.
18. Bittel, C., Tabares, L. C., Armesto, M., Carrillo, N., and Cortez, N. (2003) The oxidant-responsive diaphorase of *Rhodobacter capsulatus* is a ferredoxin (flavodoxin)-NADP(H) reductase, *FEBS Lett. 553*, 408−412.
19. Ingelmann, M., Bianchi, V., and Eklund, H. (1997) The three-dimensional structure of flavodoxin reductase from *Escherichia coli* at 1.7 Å resolution, *J. Mol. Biol. 268*, 147−157.
20. Sridhar, P. G., Kresge, N., Muhlberg, A. B., Shaw, A., Jung, Y. S., Burgess, B. K., and Stout, C. D. (1998) The crystal structure of NADPH:ferredoxin reductase from *Azotobacter vinelandii*, *Protein Sci. 7*, 2541−2549.
21. Batie, C. J., and Kamin, H. (1984) Electron transfer by ferredoxin-$NADP^+$ reductase. Rapid-reaction evidence for participation of a ternary complex, *J. Biol. Chem. 259*, 11976−11985.
22. Zeilstra-Ryalls, J. H., and Kaplan, S. (2004) Oxygen intervention in the regulation of gene expression: the photosynthetic bacterial paradigm, *Cell. Mol. Life Sci. 61*, 417−436.
23. Armengaud, J., Meyer, C., and Jouanneau, Y. (1997) A [2Fe-2S] ferredoxin (FdVI) is essential for growth of the photosynthetic bacterium *Rhodobacter capsulatus*, *J. Bacteriol. 179*, 3304−3309.
24. Saeki, K., Suetsugu, Y., Tokuda, K., Miyatake, Y., Young, D. A., Marrs, B. L., and Matsubara, H. (1991) Genetic analysis of functional differences among distinct ferredoxins in *Rhodobacter capsulatus*, *J. Biol. Chem. 266*, 12889−12895.
25. Medina, M., Martínez-Júlvez, M., Hurley, J. K., Tollin, G., and Gómez-Moreno, C. (1998) Involvement of Glutamic 301 in the catalytic mechanism of ferredoxin-$NADP^+$ reductase from *Anabaena* PCC 7119, *Biochemistry 37*, 2715−2728.
26. Mayhew, S. G. (1999) Potentiometric Measurement of Oxidation−reduction Potentials, in *Flavoprotein Protocols* (Chapman, S. K., and Reid, G. A., Eds.) pp 49−59, Humana Press, Totowa, NJ.
27. Pérez-Dorado, I., Bittel, C., Cortez, N., and Hermoso, J. A. (2004) Crystallization and preliminary X-ray diffraction analysis of ferredoxin-NADP(H) reductase from *Rhodobacter capsulatus*, *Acta Crystallogr. D 60*, 2332−2335.
28. Leslie, A. G. W. (1987) Profile Fitting, in *Proceedings of the CCP4 Study Weekend* (Machin, J. R., and Papiz, M. Z., Eds.) pp 39−50, SERC Daresbury Laboratory, Warrington.
29. Bailey, S. (1994) The *CCP*4 suite: programs for protein crystallography, *Acta Crystallogr. D 50*, 760−763.
30. Navaza, J. (1994) *AMoRe*: an automated package for molecular replacement, *Acta Crystallogr. A 50*, 157−163.
31. Brunger, A. T., Adams, P. D., Clore, G. M., DeLano, W. L., Gros, P., Grosse-Kunstleve, R. W., Jiang, J. S., Kuszewski, J., Nilges, M., Pannu, N. S., Read, R. J., Rice, L. M., Simonson, T., and Warren, G. L. (1998) Crystallography and NMR system: a new software suite for macromolecular structure determination, *Acta Crystallogr. D 54*, 905−921.
32. Jones, T. A., Zou, J. Y., Cowan, S. W., and Kjeldgaard, M. (1991) Improved methods for building protein models in electron density maps and the location of errors in these models, *Acta Crystallogr. A 47*, 110−119.
33. Laskowski, R. A., MacArthur, M. W., Moss, D. S., and Thornton, J. M. (1993) *PROCHECK*: a program to check the stereochemical quality of protein structures, *J. Appl. Crystallogr. 26*, 283−291.
34. Hooft, R. W. W., Vriend, G., Sander, C., and Abola, E. E. (1996) Errors in protein structures, *Nature 381*, 272.

35. Kraulis, P. J. (1991) *SCRIPT*: a program to produce both detailed and schematic plots of protein structures, *J. Appl. Crystallogr. 24*, 946−950.
36. Nicholls, A., and Honig, B. A. (1991) Rapid finite difference algorithm, utilizing succesive over-relaxation to solve the Poisson−Boltzmann equation, *J. Comput. Chem. 12*, 435−445.
37. Holm, L., and Sander, C. (1996) The FSSP database: fold classification based on structure-structure alignment of proteins, *Nucleic Acids Res. 24*, 206−209.
38. Hermoso, J. A., Mayoral, T., Faro, M., Gómez-Moreno, C., Sanz-Aparicio, J., and Medina, M. (2002) Mechanism of coenzyme recognition and binding revealed by crystal structure analysis of ferredoxin-$NADP^+$ reductase complexed with $NADP^+$, *J. Mol. Biol. 319*, 1133−1142.
39. Deng, Z., Aliverti, A., Zanetti, G., Arakaki, A. K., Ottado, J., Orellano, E. G., Calcaterra, N. B., Ceccarelli, E. A., Carrillo, N., and Karplus, P. A. (1999) A productive $NADP^+$ binding mode of ferredoxin-$NADP^+$ reductase revealed by protein engineering and crystallographic studies, *Nat. Struct. Biol. 6*, 847−853.
40. Nogués, I., Tejero, J., Hurley, J. K., Paladini, D., Frago, S., Tollin, G., Mayhew, S. G., Gómez-Moreno, C., Ceccarelli, E. A., Carrillo, N., and Medina M. (2004) Role of the carboxyl-terminal tyrosine of ferredoxin-$NADP^+$ reductase in the electron transfer processes with the protein carriers ferredoxin and flavodoxin, *Biochemistry 43*, 6127−6137.
41. Corrado, M. E., Aliverti, A., Zanetti, G., and Mayhew, S. G. (1996) Analysis of the oxidation−reduction potentials of recombinant ferredoxin-$NADP^+$ reductase from spinach chloroplasts, *Eur. J. Biochem. 239*, 662−667.
42. Hallenbeck, P. C., and Gennaro, G. (1998) Stopped-flow kinetic studies of low potential electron carriers of the photosynthetic bacterium *Rhodobacter capsulatus*: ferredoxin I and NifF, *Biochim. Biophys. Acta 1365*, 435−442.
43. McIver, L., Leadbeater, C., Campopiano, D., Baxter, R. L., Daff, S. N., Chapman, S. K., and Munro, A. W. (1998) Characterisation of flavodoxin $NADP^+$ oxidreductase and flavodoxin; key components of electron transfer in *Escherichia coli*, *Eur. J. Biochem. 257*, 577−585.
44. Wan, J. T., and Jarrett, J. T. (2002) Electron acceptor specificity of ferredoxin (flavodoxin):$NADP^+$ oxidoreductase from *Escherichia coli*, *Arch. Biochem. Biophys. 406*, 116−126.
45. Murataliev, M. B., Feyereisen, R., and Walker, F. A. (2004) Electron transfer by diflavin reductases, *Biochim. Biophys. Acta 1698*, 1−26.
46. Sevrioukova, I., Shaffer, C., Ballou, D. P., and Peterson, J. A. (1996) Equilibrium and transient state spectrophotometric studies of the mechanism of reduction of the flavoprotein domain of P450BM-3, *Biochemistry 35*, 7058−7068.
47. Fu, J., Yamamoto, K., Guan, Z. W., Kimura, S., and Iyanagi, T. (2004) Human neuronal nitric oxide synthase can catalyze one-electron reduction of adriamycin: role of flavin domain, *Arch. Biochem. Biophys. 427*, 180−187.
48. Masters, B. S. S., Kamin, H., Gibson, Q. H., and Williams, C. H., Jr. (1965) Studies on the mechanism of microsomal triphosphopyridine nucleotide-cytochrome *c* reductase, *J. Biol. Chem. 240*, 921−931.
49. Jenkins, C. M., and Waterman, M. R. (1994) Flavodoxin and NADPH-flavodoxin reductase from *Escherichia coli* support bovine cytochrome P450 c17 hydroxylase activities, *J. Biol. Chem. 269*, 27401−27408.
50. Jenkins, C. M., Genzor, C. G., Fillat, M. F., Waterman, M. R., and Gómez-Moreno, C. (1997) Negatively charged *Anabaena* flavodoxin residues (Asp144 and Glu145) are important for reconstitution of cytochrome P450 17 α-hydroxylase activity, *J. Biol. Chem. 272*, 22509−22513.
51. Mayhew, S. G., and Tollin, G. (1993) General Properties of Flavodoxins, in *Chemistry and Biochemistry of Flavoenzymes* (Müller, F., Ed.) pp 389−426, CRC Press, Boca Raton, FL.

BI0508183